Design and Measurements of Mach-Zedner Interferometer using Silicon on Insulator Photonics Process

Youssef Rachad - yr_9

***Abstract*—Mach-Zedner interferometers are devices used in silicon photonics for optical modulation and sensors. In this report, a Mach-Zedner interferometer was designed using the KLayout software a parameter variations are introduced to study the effects of path length differences on the FSR and the group index of the interferometer. Simulation results are obtained using the LUMERICAL solver and demonstrate good agreement with theoretical models. Fabrication of the devices was done at the Washington Nanofabrication Facility and the measurements were automated at the UBC Photonics Research Group labs. We can also try out a ring resonator and see that it has a better defined FSR.**

I. Introduction

Photonics integrated circuits (PIC) have gained significant traction due to their high speed applications and increasing demand in optical networking. An essential component to optical circuits is the interferometer and among them, the Mach-Zehnder interferometer (MZI) presents a simple applications of photonics. The MZI is a fundamental component in developing complex silicon-photonics ICs and its simplicity lends itself to complex applications and comprehensive characterisations. The MZI can be found in applications such as optical modulation, multiplexing and optical switching and optical routing.

This paper will focus on the fabrication of MZI using the so called silicon-on-insulator (SOI) technology which is easily and reliably fabrication using an electron beam lithography (EBL) process.

II. Theory

The MZI exploits the path length difference between two split beams from a source to produce BOZO interference effect. The designed device consists of 3 main components:

- Diffraction gratings, used both as input source of polarised light and as output ports during measurements
- Y-Beam splitters used in this implementation to splitting the incoming light in a 1:1 ratio, and
- Strip waveguides designed to support single mode propagation. This implementation compares $1550[\mathrm{nm}]$ TE and $1550[\mathrm{nm}]$ TM polarisations.

A. Diffraction Grating Coupler

Diffraction gratings implement surface coupling to input light into the silicon photonics chip. When light enters the diffraction grating coupler from the optical fibre, it diffracts off of the periodic mechanical structure such that the resulting wavelength is determined by the periodicity of the grating.

B. Strip Waveguides

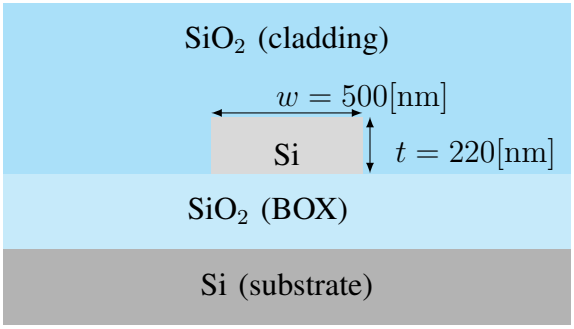

Figure 1: Strip waveguide geometry of the SOI technology. The waveguide is made of silicon and has a width w, of $500[\mathrm{nm}]$ and a thickness t, of $220[\mathrm{nm}]$.

Waveguides are electronic structure akin to electrical wires in that they propagate the input light

throughout the circuit and serve to connect the various components in the PIC. Waveguides can be described by their phase and group indices which indicate the phase and group velocities at which a particular wavelength or packet of light travels in the structure. The waveguides used in this BOZO experiment have a strip waveguide geometry and are $220[\mathrm{nm}$ thick by $500[\mathrm{nm}$ wide.

Waveguides allow for the propagation of light plane wave of the form

$$E = E_0 \exp(-\imath\beta L)$$

where $\beta = \frac{2\pi n}{\lambda}$ is the propagation constant

An essential technique in silicon photonics design is to bend waveguides and enable complex designs. However, the bend structures in an optical path introduce additional scattering of the light and leads to both radiation losses and mode mismatches that reduce the intensity of the fundamental mode of propagation. The mode mismatch is observed as an asymmetry in the mode profile with respect to the waveguide cross section. The result is that second and further modes will be observed during the propagation of light. Additionally, radiation losses are observed as portions of the light seen leaking/escaping out of the waveguide structure hence some of the light is lost out of the system.

The key parameter of waveguide bends is their bend radius which determines the losses incurred during the bend as well as the difficulty by which the additional modes are filtered out downstream. A larger bend radius is observed to reduce losses and in this implementation, a bend radius of $5[\mu\mathrm{m}]$ is observed to produce negligible losses - acting almost as a locally straight structure.

C. Y-Beam Splitter

Y-Beam components can be used to split an incoming plane wave into 2 plane waves or to join 2 incoming plane waves into a single output wave via interference. In this implementation BOZO, Y-Beam splitters are used to split an incoming plane wave into 2 equal outputs. By assumption the Y-Beam is symmetric and the waveguide entering has uniform energy density, hence the intensity is equally split into two parts

$$I_1 = I_2 = \frac{I_0}{2}$$

D. Mach-Zehndner Interferometer

The interferometer is characterised by its transfer function which describes the gain in intensity at the output given some input light. The lossless transfer function for an imbalanced interferometer of homogenous structure is given by

$$\frac{I_o}{I_i} = \frac{1}{2}\left(1 + \cos(\phi)\right) = \frac{1}{2}\left(1 + \cos\left(\frac{2\pi n_{\text{eff}}\Delta L}{\lambda}\right)\right),$$

where the phase term $\phi = \beta\Delta L$ is proportional to the propagation constant and the OPL difference in the interferometer.

1) Theoretical Derivation for MZI FSR and n_g: Another essential property of an MZI design is its free spectral range (FSR) and the group index which can be derived from the MZI transfer function.

We seek an expression for the free spectral range which measures the distance between two adjacent peaks in the transmission spectrum: FSR $= \Delta\lambda$.

We note that the phase difference between adjacent peaks is given by $\Delta\phi = 2\pi \implies \Delta\beta = \frac{2\pi}{\Delta L}$. Now we assume that the change in propagation constant and in the wavelength are proportional to one another to write

$$\Delta\beta \approx -\frac{\mathrm{d}\beta}{\mathrm{d}\lambda}\Delta\lambda.$$

Using the definition of the propagation constant, we can find

$$\frac{\mathrm{d}\beta}{\mathrm{d}\lambda} = \frac{2\pi}{\lambda}\frac{\mathrm{d}n_{\text{eff}}}{\mathrm{d}\lambda} - \frac{2\pi n_{\text{eff}}}{\lambda^2} \tag{1}$$

$$= -\frac{2\pi}{\lambda^2}\left(n_{\text{eff}} - \lambda\frac{\mathrm{d}n_{\text{eff}}}{\mathrm{d}\lambda}\right) \tag{2}$$

We can thus define the group velocity to be

$$n_g = n_{\text{eff}} - \lambda\frac{\mathrm{d}n_{\text{eff}}}{\mathrm{d}\lambda},$$

and obtain

$$\Delta\lambda = \frac{1}{\Delta L}\left(\lambda^2 \cdot \frac{1}{n_g}\right).$$

Therefore we obtain

$$n_g = \frac{\lambda^2}{\text{FSR} \cdot \Delta L}$$

III. Modelling and Simulation

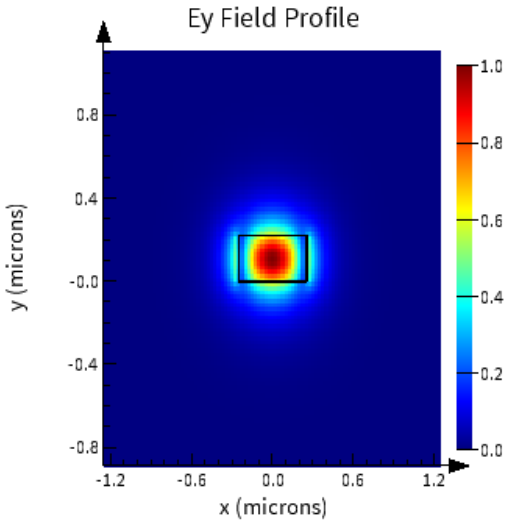

(a) TE y components of E-field intensity.

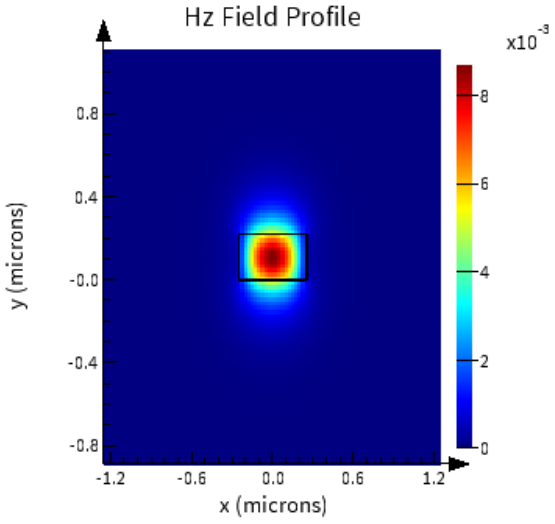

(b) TE z component of H-field intensity.

Figure 2: First quasi-TE mode profile for the chosen geometry simulated in the LUMERICAL MODE solver.

The waveguide structure was simulated using the LUMERICAL MODE eigensolver [8] to determine the mode profiles of the SOI technology. The waveguide cross section is defined according to the appropriate geometry of 500nm in width (in the x-dimension) and 220nm in height (in the y-dimension) as described in Figure 1. The silicon oxide and buried silicon oxide is defined to occupy the remainder of the geometry and the simulation space is taken within the oxide volume and defined far away enough from the silicon core to ensure the metal boundary conditions do not incur reflections [7] that degrade the simulation accuracy. Both the first TE and TM modes are simulated for a central wavelength of 1550nm and their mode profiles are illustrated in Figures 2 and 3.

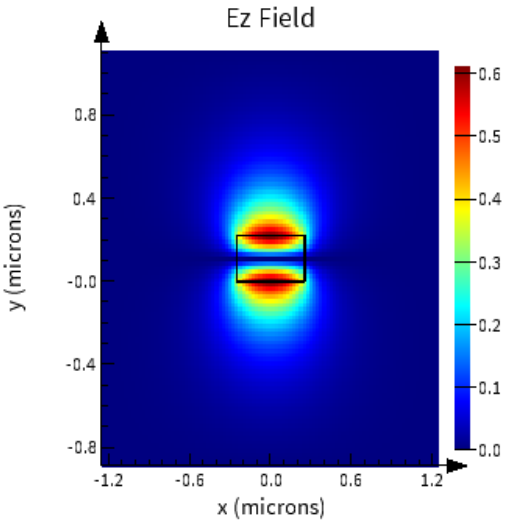

(a) TM z components of E-field intensity.

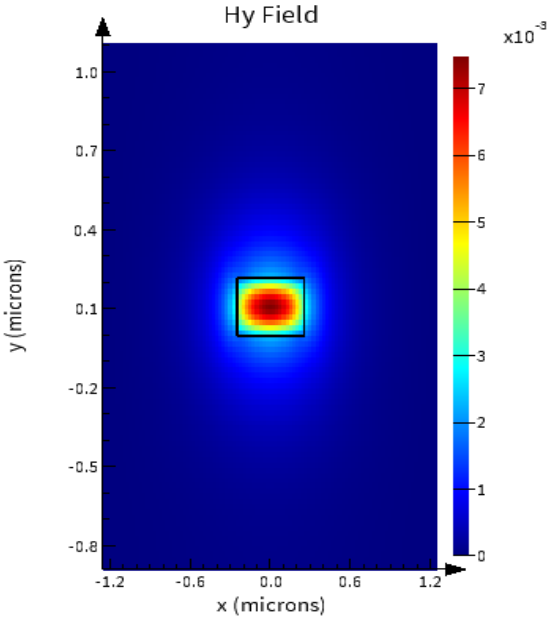

(b) TM y component of H-field intensity.

Figure 3: First quasi-TM mode profile for the chosen geometry simulated in the LUMERICAL MODE solver.

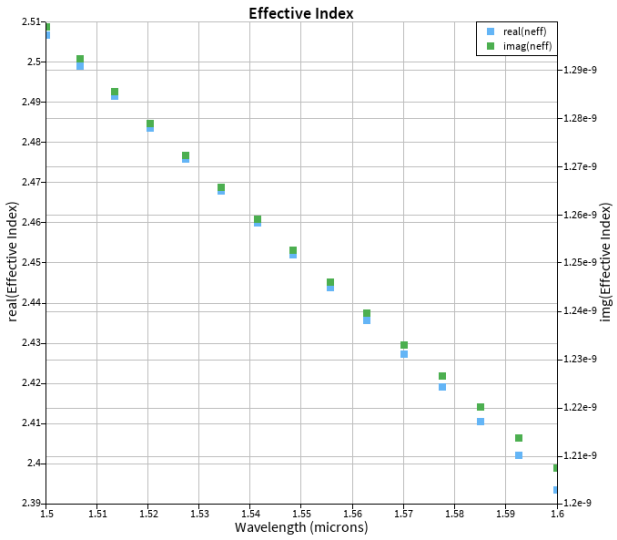

(a) Effective index of refraction as a function of wavelength.

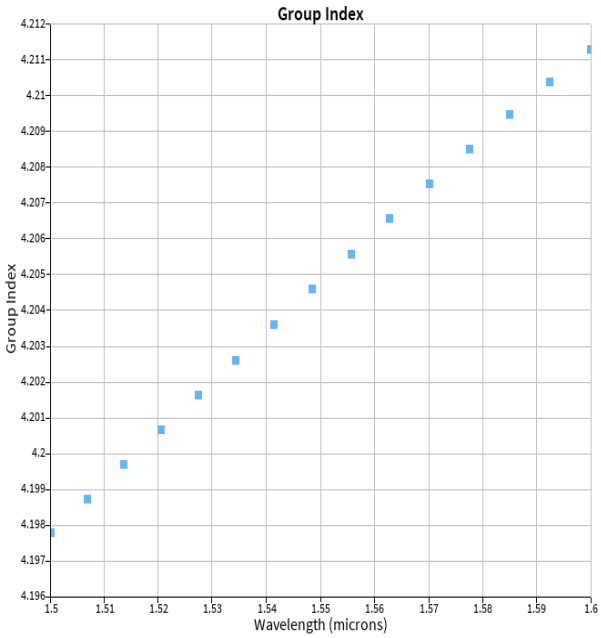

(b) Group index as a function of wavelength.

Figure 4: First quasi-TE mode profile for the chosen geometry simulated in the LUMERICAL MODE solver.

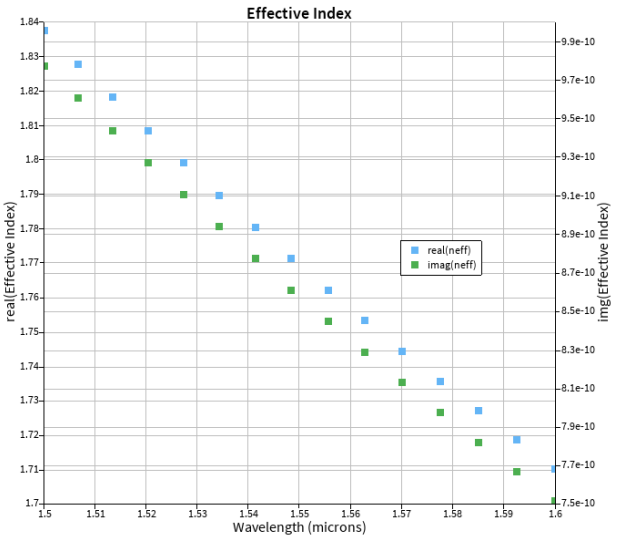

(a) Effective index of refraction as a function of wavelength.

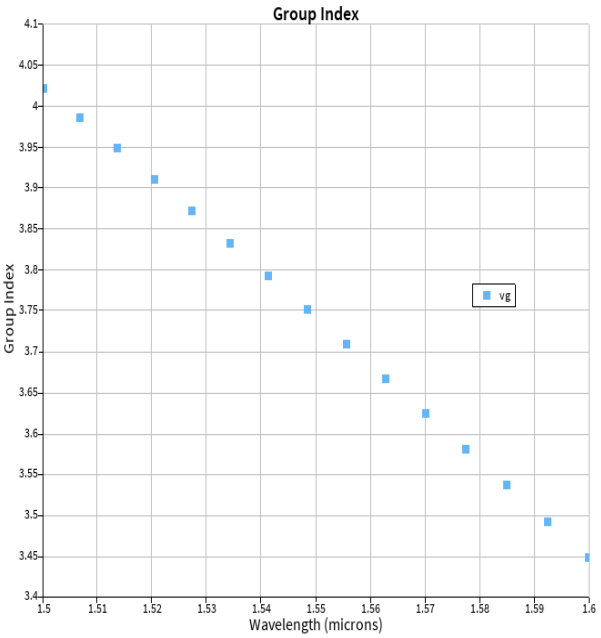

(b) Group index as a function of wavelength.

Figure 5: First quasi-TM mode profile for the chosen geometry simulated in the LUMERICAL MODE solver.

The effects of bend radius on the total loss were also modeled to confirm a design decision to use a radius of 5um in the MZI devices.

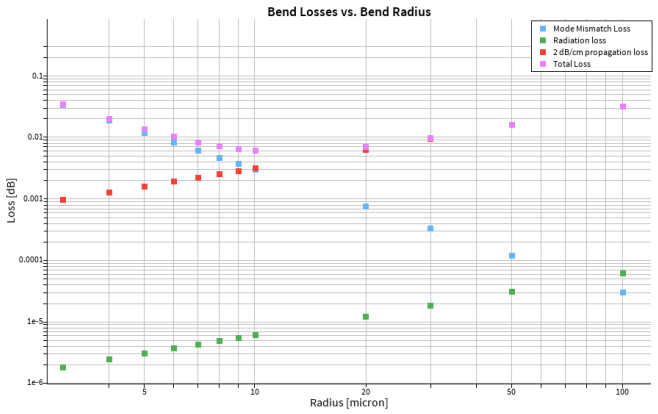

Figure 6: Total losses in a TE waveguide as a function of bend radius. Note that the total losses are calculated as the sum of all other losses. At 5um, the total losses are around 0.01dB = 1.15% and dominated by mode mismatch losses. Further increasing the radius leads to losses dominated by scattering losses which have negative impacts on the subsequent propagation of light.

A. *Experimental Obtention of MZI FSR and n_g*

Experimentally, we can observe the peaks in the transmissio spectrum of an interferometer using `findpeaks` implementation BOZO matlab and use the above equation to find the group index at each swept wavelength value. Further, the results can be corroborated using a 2 step curve fitting method for the lossy case of the MZI transfer function

$$\frac{I_o}{I_i} = 10\log_{10}\left(\frac{1}{4}\left|1+\exp\left(-\imath\frac{2\pi n_{\text{eff}}}{\lambda}\Delta L-\frac{\alpha\Delta L}{2}\right|^2\right)\right)+b.$$

Thus if we use a 2nd order truncated Taylor polynomial,

$$n_{\text{eff}}(\lambda) = n_1 + n_2(\lambda-\lambda_0) + n_3(\lambda-\lambda_0)^2,$$

where λ_0 is the central frequency ($1550[\text{nm}]$ and n_1, n_2, n_3 are the fit parameters, then we can obtain the following results

$$n_{\text{eff}} = n_1 \tag{3}$$
$$n_g = n_1 - n_2\lambda_0 \tag{4}$$

Simulating the TE mode profile yielded values $n_1 = 2.4502,\ n_2 = -1.1321,\ n_3 = -0.0413$, thus the simulated effective index is $n_{\text{eff}} = 2.4502$ and the simulated group index is 4.2049.

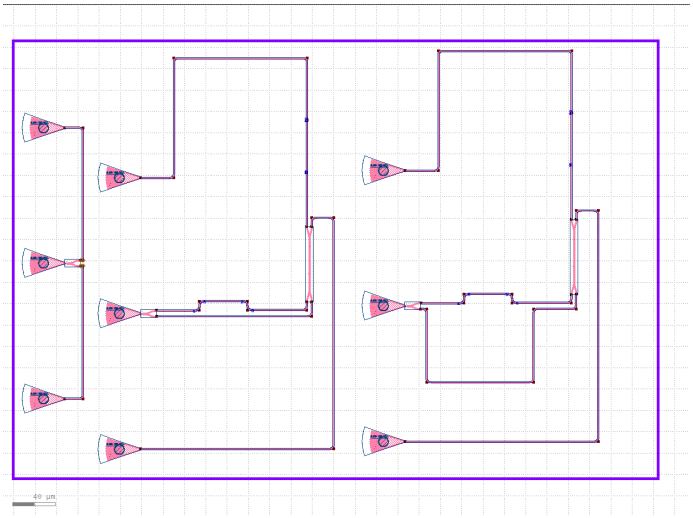

Figure 7: Tile (one of 2) containing simulated circuits to model FSR and group index.

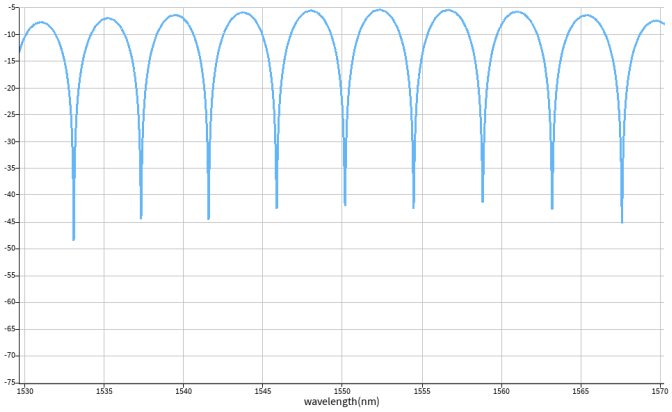

Figure 8: Transmission plot of TE MZI with OPL difference of $\Delta L = 133[\mu\text{m}]$. The plot is given as the transmission in dB vs. wavelength in nanometers.

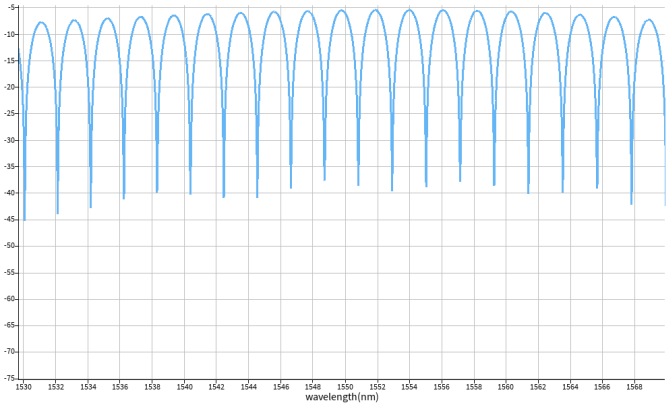

Figure 9: The plot is given as the transmission in dB vs. wavelength in nanometers.

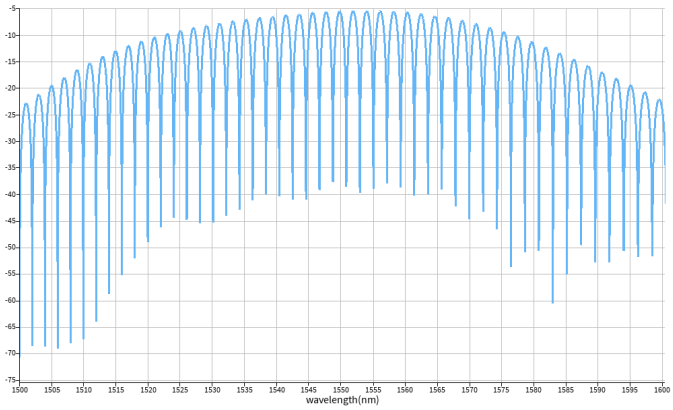

Figure 10: Transmission plot of TE MZI with OPL difference of $\Delta L = 273[\mu\text{m}]$. The plot is given as the transmission in dB vs. wavelength in nanometers. The full spectrum is displayed to show the behaivour of the MZI away from the design wavelength.

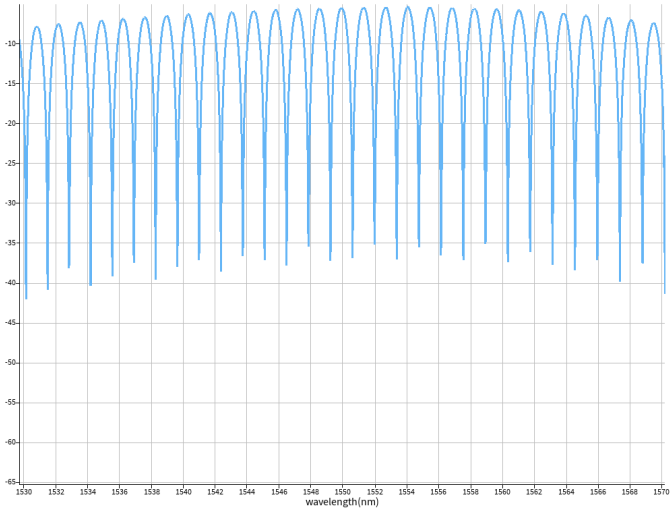

Figure 11: Transmission plot of TE MZI with OPL difference of $\Delta L = 413[\mu\text{m}]$. The plot is given as the transmission in dB vs. wavelength in nanometers.

The simulated performance is summarised in Table I

$\Delta L[\mu m]$	FSR [nm] (calculated)	n_g (calculated)
133	4.3	4.205
273	2.095	4.205
413	1.385	4.205
$\Delta L[\mu m]$	FSR [nm] (simulated)	n_g (simulated)
133	4.298	4.203
273	2.120	4.151
413	1.367	4.255

Table I: Calculated and simulated performance of the interferometers.

We can plot the calculated and the simulated FSR values for comparison and observe the OPL difference dependency.

Calculated and Simulated FSR vs. Path Length Difference

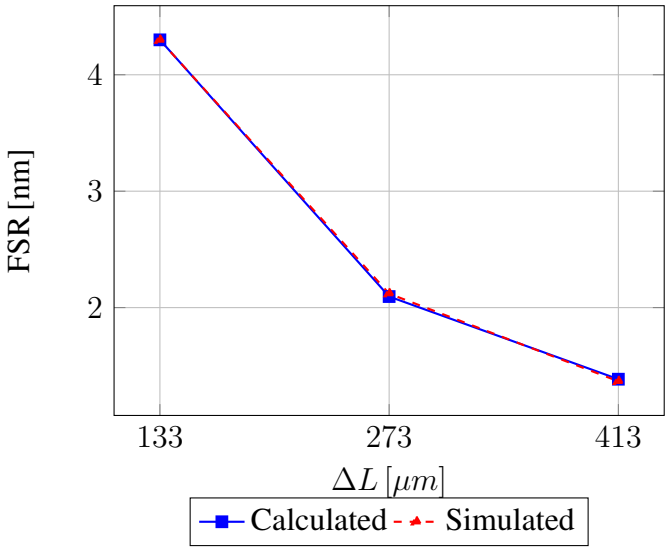

B. *Corner Analysis*

Corner analysis is carried out to simulate the expect value boudaries given known manufacturing challenges. Here we address EBeam errors by considering a variation in width and thick in the waveguide's cross section. The results are a range of group indices that represent a normal range given the process' accuracy.

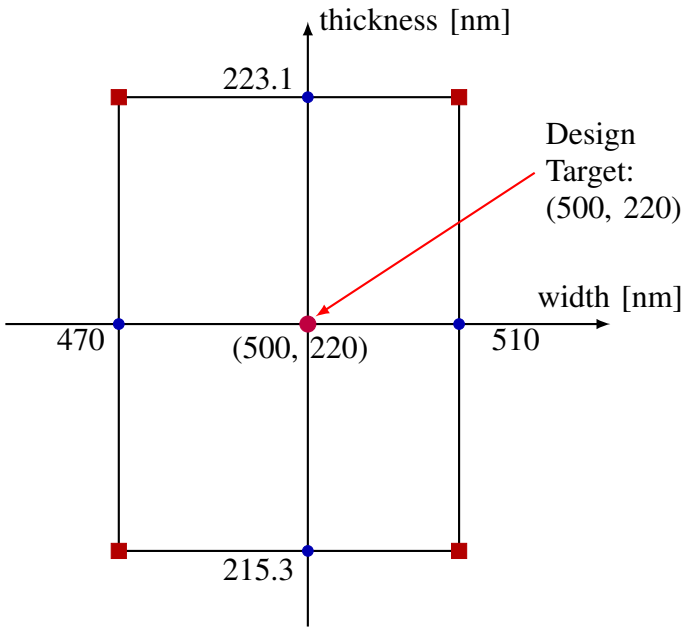

Figure 12: Corner analysis diagram centered on the targeted design dimensions. According to the wafer specification, we take the thickness to be $219.2 \pm 3.9[\mathrm{nm}]$ and the width to be $500 + 10/-30[\mathrm{nm}]$. The four corner cases (in squares) are simulated in addition to the design target.

Geometry	Mode	Effective Index n_{eff}	Group Index n_g
470×215.3	TE		
	TM		
470×223.1	TE		
	TM		
510×215.3	TE		
	TM		
510×223.1	TE		

Table II: Effective and group indices obtain from corner analysis. The largest and smallest BOZO

IV. Fabrication

The devices were fabricated at the Washington Nanofabrication Facility (WNF). Their silicon photonics process is described as follows. The devices were fabricated using 100 keV Electron Beam Lithography [1]. The fabrication used silicon-on-insulator wafer with 220 nm thick silicon on 3 um thick silicon dioxide. The substrates were 25 mm squares diced from 150 mm wafers. After a solvent rinse and hot-plate dehydration bake, hydrogen silsesquioxane resist (HSQ, Dow-Corning XP-1541-006) was spin-coated at 4000 rpm, then hotplate baked at 80 °C for 4 minutes. Electron beam lithography was performed using a JEOL JBX-6300FS system operated at 100 keV energy, 8 nA beam current, and 500 um exposure field size. The machine grid used for shape placement was 1 nm, while the beam stepping grid, the spacing between dwell points during the shape writing, was 6 nm. An exposure dose of 2800 uC/cm2 was used. The resist was developed by immersion in 25% tetramethylammonium hydroxide for 4 minutes, followed by a flowing deionized water rinse for 60 s, an isopropanol rinse for 10 s, and then blown dry with nitrogen. The silicon was removed from unexposed areas using inductively coupled plasma etching in an Oxford Plasmalab System 100, with a chlorine gas flow of 20 sccm, pressure of 12 mT, ICP power of 800 W, bias power of 40 W, and a platen temperature of 20 °C, resulting in a bias voltage of 185 V. During etching, chips were mounted on a 100 mm silicon carrier wafer using perfluoropolyether vacuum oil. Cladding oxide was deposited using plasma enhanced chemical vapor deposition (PECVD) in an Oxford Plasmalab System 100 with a silane (SiH4) flow of 13.0 sccm, nitrous oxide (N2O) flow of 1000.0 sccm, high-purity nitrogen (N2) flow of 500.0 sccm, pressure at 1400mT, high-frequency RF power of 120W, and a platen temperature of 350C. During deposition, chips rest directly on a silicon carrier wafer and are buffered by silicon pieces on all sides to aid uniformity.

V. Measurements Description

To characterize the devices, a custom-built automated test setup [2, 6] with automated control software written in Python was used [3]. An Agilent 81600B tunable laser was used as the input source and Agilent 81635A optical power sensors as the output detectors. The wavelength was swept from 1500 to 1600 nm in 10 pm steps. A polarization maintaining (PM) fibre was used to maintain the polarization state of the light, to couple the TE polarization into the grating couplers [4]. A 90º rotation was used to inject light into the TM grating couplers [4]. A polarization maintaining fibre array was used to couple light in/out of the chip [5].

VI. Experimental Results & Analysis

Below are plots of ring resonator circuits which were also designed, experimented and measured.

The raw and baseline corrected spectra are shown for TE and TM mode implementations.

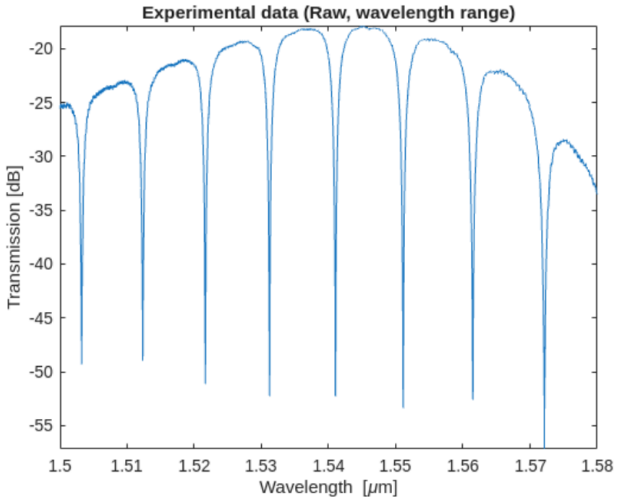

Figure 13: Raw transmission plot of TE ring resonator. The plot is given as the transmission in dB vs. wavelength in nanometers.

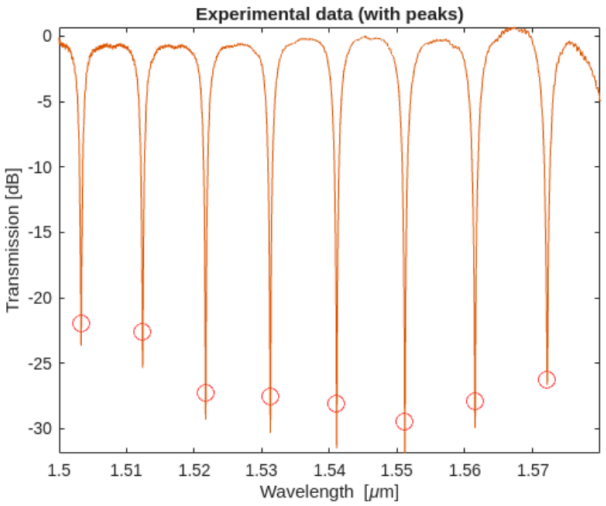

Figure 14: Baseline corrected transmission plot of TE ring resonator. The plot is given as the transmission in dB vs. wavelength in nanometers.

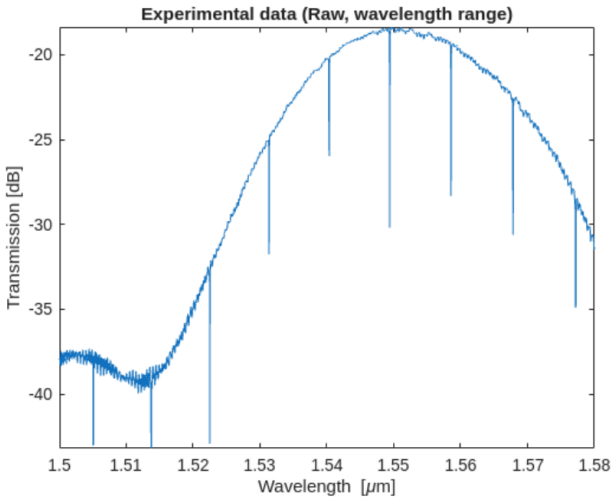

Figure 15: Raw transmission plot of TM ring resonator. The plot is given as the transmission in dB vs. wavelength in nanometers.

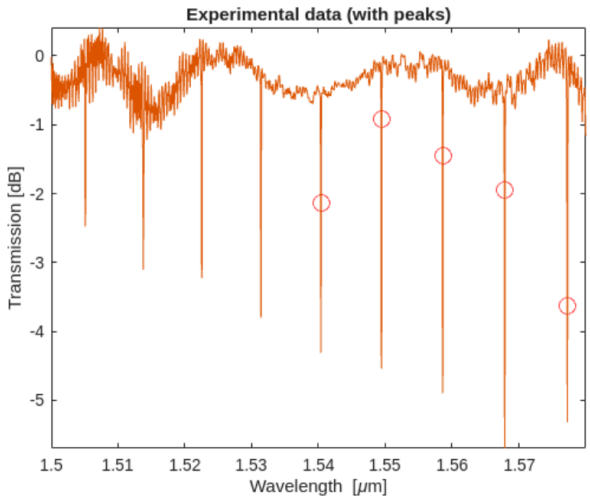

Figure 16: Baseline corrected transmission plot of TM ring resonator. The plot is given as the transmission in dB vs. wavelength in nanometers.

Further analysis such as taking the difference in peaks will lead to FSR value computation.

VII. Acknowledgments

I acknowledge the edX UBCx Phot1x Silicon Photonics Design, Fabrication and Data Analysis course, which is supported by the Natural Sciences and Engineering Research Council of Canada (NSERC) Silicon Electronic-Photonic Integrated Circuits (SiEPIC) Program. The devices were fabricated by Richard Bojko at the University of Washington Washington Nanofabrication Facility,

part of the National Science Foundation's National Nanotechnology Infrastructure Network (NNIN), and Cameron Horvath at Applied Nanotools, Inc. Omid Esmaeeli performed the measurements at The University of British Columbia. We acknowledge Lumerical Solutions, Inc., Mathworks, Mentor Graphics, Python, and KLayout for the design software.

VIII. References

[1] R. J. Bojko, J. Li, L. He, T. Baehr-Jones, M. Hochberg, and Y. Aida, "Electron beam lithography writing strategies for low loss, high confinement silicon optical waveguides," J. Vacuum Sci. Technol. B 29, 06F309 (2011)

[2] Lukas Chrostowski, Michael Hochberg, chapter 12 in "Silicon Photonics Design: From Devices to Systems", Cambridge University Press, 2015

[3] http://siepic.ubc.ca/probestation, using Python code developed by Michael Caverley.

[4] Yun Wang, Xu Wang, Jonas Flueckiger, Han Yun, Wei Shi, Richard Bojko, Nicolas A. F. Jaeger, Lukas Chrostowski, "Focusing sub-wavelength grating couplers with low back reflections for rapid prototyping of silicon photonic circuits", Optics Express Vol. 22, Issue 17, pp. 20652-20662 (2014) doi: 10.1364/OE.22.020652

[5] www.plcconnections.com, PLC Connections, Columbus OH, USA.

[6] http://mapleleafphotonics.com, Maple Leaf Photonics, Seattle WA, USA.

[7] D. K. Cheng, Field and Wave Electromagnetics, 2nd ed. Reading, MA, USA: Addison-Wesley, 1989.

[8] Lumerical, Ansys Inc., 2025. [Software]. Available: https://www.lumerical.com/products/